

Aircraft failure detection and identification over an extended flight envelope using an artificial immune system

H. Moncayo

M. G. Perhinschi

mario.perhinschi@mail.wvu.edu

J. Davis

West Virginia University

West Virginia

USA

ABSTRACT

An integrated artificial immune system-based scheme that can operate over extended areas of the flight envelope is proposed in this paper for the detection and identification of a variety of aircraft sensor, actuator, propulsion, and structural failures/damages. A hierarchical multi-self strategy has been developed in which different self configurations are selected for detection and identification of specific abnormal conditions. Data collected using a motion-based flight simulator were used to define the self for a wide area of the flight envelope and to test and validate the scheme. The aircraft model represents a supersonic fighter, including model-following direct adaptive control laws based on non-linear dynamic inversion and artificial neural network augmentation. The proposed detection scheme achieves low false alarm rates and high detection and identification rates for all the categories of failures considered.

NOMENCLATURE

B	state space system control matrix
DQEE _x	decentralised quadratic estimation error
<i>e</i>	estimation error
e	tracking error
\hat{f}	invertible approximation of <i>f</i>
K_a, K_p, K_d	gains of a proportional-integral-derivative type controller
K_D, K_P, K_I	gain matrices
L_f, M_f, N_f	non-linear terms of the moment equations
MQEE	main quadratic estimation error
NMOV	number of smallest rejected detectors to be moved
$NN_{w(x)}$	specific neural network weight

NN_{outx}	specific neural network output
NRD	number of random centres
OQEE	output quadratic estimation error
<i>p, q, r</i>	measured roll, pitch, and yaw rates, [rad/sec]
$P_{ref}, q_{ref}, r_{ref}$	reference angular rates
$\hat{P}_{DNN}, \hat{q}_{DNN}, \hat{r}_{DNN}$	neural estimates of angular rates that do not include the respective gyro
$\hat{P}_{MNN}, \hat{q}_{MNN}, \hat{r}_{MNN}$	neural estimates of angular rates that include the respective gyro
R_{pq}	roll-pitch cross correlation coefficient
R_{rr}	yaw auto correlation coefficient
u	control vector
$U_{Pads}, U_{qads}, U_{rad}$	augmentation commands generated by artificial neural networks
x	state vector, input vector
x_{TE}	angular rate tracking error [rad/sec]
Δ	error associated with \hat{f}
$\delta_a, \delta_e, \delta_r$	control surface deflections
$\delta_{acom}, \delta_{ecom}, \delta_{rcom}$	Control surface commands
$\delta_{lonstick}$	longitudinal stick displacement
$\delta_{latstick}$	lateral stick displacement
$\delta_{divpedal}$	pedal displacement
θ	set of parameters to be tuned by the learning algorithm
μ	Gaussian centre positions
v	pseudo-control
σ	variances
ω	detection time window

1.0 INTRODUCTION

The timely detection of abnormal flight conditions and reliable automatic compensation can drastically increase the safety of aircraft operations. Therefore, the availability of failure detection and identification (FDI) schemes with high rates of success, with comprehensive coverage over the entire flight envelope, and integrating all aircraft sub-systems and operational modes is a critical objective that has been widely acknowledged⁽¹⁻⁵⁾.

Research efforts in this area to date have focused on individual classes of failures and isolated abnormal conditions at single operational points. State estimation or observer-based schemes have been widely proposed⁽⁶⁻⁹⁾ for actuator FDI relying on Kalman or other classes of filters. Artificial neural networks (NN) have been extensively used⁽¹⁰⁻¹³⁾ to solve the FDI problem for aerospace systems. Alternative approaches for FDI and pilot awareness enhancement based on inductive learning⁽¹⁴⁾ were also proposed. The issue of sensor FDI has been addressed to a lesser extent, since triple and quadruple physical redundancy of aircraft sensors is a common practice. However, sensor FDI schemes based on NN estimations of sensor outputs have been proposed^(15,16). Research regarding the dynamic impact and accommodation of structural damage to main aircraft components (wing, horizontal tail) has recently focused upon the development of fault-tolerant control laws⁽¹⁷⁾ with indirect failure assessment through parameter identification without explicit FDI. The use of large networks of sensors for global structural health monitoring has also been investigated⁽¹⁸⁾. Regulations require that multiple engine aircraft be capable of safe operation if one engine fails. In such situations, a detection scheme could provide useful information that is necessary for the pilot and the control system regarding the occurrence of the failure, location, and evaluation of the effect on reducing the flight envelope.

The attempt to integrate FDI for a large diversity of aircraft sub-systems and over extended areas of the flight envelope poses significant challenges. From a failure accommodation point of view, the differentiation between – for example – a sensor and an actuator failure is a critical task because different types of compensation are necessary in each case. If the specific signal associated with the sensor failure is used in the control laws, it might be challenging for a pilot to distinguish between sensor and actuator failures. Furthermore, very often, it is important but difficult to determine – within each of the two categories – which particular element has failed. Such issues related to the integration of FDI for different classes of failure have only been addressed on a limited basis⁽¹⁶⁾ and comprehensive and systematic methodologies have yet to be developed.

The complexity and extremely high dimensionality of the FDI problem for aircraft sub-systems require adequate tools. In

particular, the multi-dimensionality of the parameter space associated with the dynamic response of the aircraft at abnormal conditions exposes the FDI process to specific issues with potential negative impact. Recently, a new concept inspired from the biological immune system was proposed for aerospace systems FDI^(19,20). The Artificial Immune System (AIS)-based fault detection operates in a similar manner to its biological counterpart – according to the principle of self/non-self discrimination – when it distinguishes between entities that belong to the organism (self) and entities that do not (non-self). All appropriate parameters must be identified that are capable of capturing the dynamic signatures of each type of failure considered. Therefore, these parameters characterise/define the ‘self’ – or normal conditions – and, for that matter, the non-self – or the abnormal conditions. The concept of immunity-based fault detection originates from the idea that an abnormal situation can be declared when a current configuration of ‘features’ or ‘identifiers’ matches with a configuration from a pre-determined set – detectors – known NOT to correspond to a normal situation.

An integrated set of methodologies for AIS-based detection, identification, and evaluation of a wide variety of aircraft sensor, actuator, propulsion, and structural failures/damages has been developed⁽²¹⁾ at West Virginia University (WVU) within NASA’s Aviation Safety Program. As part of this effort, the development of an integrated high-performance AIS-based FDI scheme using a hierarchical multi-self strategy is presented in this paper. The scheme is capable of detecting and identifying several categories of sub-system abnormal conditions over an extended area of the flight envelope. The effectiveness of the approach in terms of high detection rate and low number of false alarms for the four categories of failures is tested using data from the WVU motion-based flight simulator. The aircraft model represents a supersonic fighter including model-following direct adaptive control laws based on non-linear dynamic inversion and artificial neural network augmentation⁽²²⁾.

A brief review of the AIS paradigm and its application is presented in Section II. The general framework for the development and testing of the AIS-based FDI scheme is discussed in Section III including aircraft sub-system failure modelling, adaptive control laws, and motion-based flight simulator tests for self definition and performance evaluation. The design of the AIS, including data processing and detector generation and optimisation, is described in Section IV. The design process of the proposed AIS-based FDI scheme is outlined in Section V. Test results, analysis, and evaluation of the FDI scheme performance are presented in Section VI. Finally, some conclusions are summarised in Section VII followed by acknowledgements and a bibliographical list.

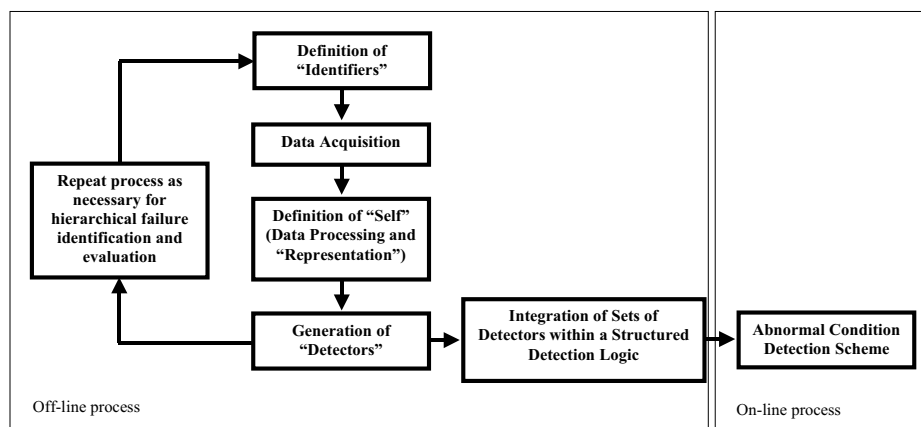


Figure 1. Artificial immune system-based abnormal condition detection.

2.0 THE ARTIFICIAL IMMUNE SYSTEM PARADIGM FOR FAULT DETECTION

The mechanisms and processes of the biological immune system are the inspiration for the AIS as a new artificial intelligence technique for fault detection⁽²³⁻²⁵⁾. In living organisms, specialised cells – T-cells⁽²⁶⁾ – are generated such that they do NOT match (negative selection⁽²⁰⁾) specific ‘features’ of the organism cells, coded as strings of proteins and polysaccharides. However, they can match intruding agents and mark them for destruction. Applying this paradigm to aircraft sub-system FDI requires that a set of adequate ‘features’ be defined. These ‘features’ can include various sensor outputs, state estimates, statistical parameters, or any other information expected to be relevant to the behaviour of the system and able to capture the signature of abnormal situations. Extensive experimental data are necessary to determine the ‘self’ or the hyperspace of normal conditions. Adequate numerical representations of the self/non-self must be used and the data processed such that they are manageable, given the computational and storage limitations of the available hardware. The artificial antibodies – the detectors – must then be generated and optimised. This process may be repeated to generate several sets of detectors for different self configurations. At this point, the obtained selves can be organised and classified based on the capability of each one to detect and identify every type of failure. Finally, a detection logic must be designed for real-time operation with high detection rates and a low number of false alarms. The block diagram of the general AIS design process⁽²¹⁾ for fault detection is presented in Fig. 1.

3.0 FRAMEWORK FOR FDI SCHEME DEVELOPMENT AND TESTING

3.1 Description of the failure modelling

Four types of failures were modelled to support the development and testing of the FDI scheme: actuator, sensor, propulsion, and structural failures/damages. A brief description of the modelling approach is presented next.

3.1.1 Actuator failure and control surface damage modelling

Within this category, failure on left or right individual stabilator, aileron, or rudder – since the aircraft considered is equipped with a dual fin – have been considered. Two types of control surface failure are modelled: stuck aerodynamic control surface and physically damaged aerodynamic control surface. The first failure type corresponds to an actuator mechanism failure and results in a locked surface; in fact, at the failure occurrence, the control surface remains fixed in the current position/deflection or moves to a pre-defined position and remains fixed there. A failure involving a blockage of the control surface at a fixed deflection does not alter the aerodynamic properties of the control surface. However, each surface in a pair (left and right) will have different deflections and the resulting moments and forces are computed individually. The second failure type corresponds to a physical destruction and/or deformation of the control surface. It consists of a deterioration of the aerodynamic control power of the control surface starting at the failure occurring moment. A control failure that involves physical damage of the control surface may alter the aerodynamic properties in manners that can be both qualitative (affecting the nature of the aerodynamic phenomena involved) and quantitative (affecting the magnitude of characteristic parameters). More details and complete models are presented in the references^(27,28).

3.1.2 Sensor failure modelling

Failures of the gyros on the three channels have been considered within this category because their outputs are used within the control laws. The simulated sensor failure implemented consists of an output bias. The transition to the biased sensor output can be instantaneous (step bias) or over a certain transient (drifting bias). Different transients as well as different sizes of the bias can be defined. Thus, two types of sensor failures are implemented: large step bias and large fast drifting bias in the angular rate sensors⁽²⁸⁾.

3.1.3 Aerodynamic surface damage modelling

For the purpose of this paper, only the damage of the wing is modelled separately. Damages to other aerodynamic surfaces may be considered as failures of the respective actuators (loss of aerodynamic control power). A simple model of wing damage is developed considering both aerodynamic and gravimetric effects. The failure type corresponds to a total or partial physical destruction and/or deformation of the wing and different percent values along the wing can be selected as damage affected area.

3.1.4 Engine failure modelling

Simple models for the following engine failures/malfunctions have been implemented: stuck throttle, thrust runaway, and power/thrust reduced control efficiency. The ‘stuck throttle’ failure implies normal operation of the engine but no response to power lever actuation. The ‘thrust runaway’ failure models a malfunction of the fuel control system, which causes the increase of the fuel flow to maximum and the increase of the thrust as a result. This is modelled by increasing the throttle to maximum with first order dynamics and time constant set-up by the user. Finally, the ‘power/thrust reduced control efficiency’ is modelled by scaling down the throttle input by a constant factor selected by the user. For this paper, only the latter type of engine failure is considered.

3.2 Aircraft model and adaptive control laws

The aircraft aerodynamic model used was derived from a non-linear model of a high performance military aircraft distributed by NASA to academic institutions in 1990 within a student design competition⁽²⁹⁾. This generic model was customised through the addition of the aerodynamics modelling of canard surfaces for the purpose of simulating the NASA IFCS F-15 research aircraft⁽²²⁾. The aerodynamic and thrust characteristics are provided through 42 look-up tables. The look-up tables have been subdivided to isolate the contribution of individual aerodynamic surfaces, control surfaces, and engines in order to be able to simulate structural damage, control surface failure, and engine malfunction.

The direct adaptive control laws use a ‘model following’ architecture based on non-linear dynamic inversion (NLDI) augmented with artificial neural networks (NN). This architecture, presented in Fig. 2, has shown capabilities for compensating tracking errors while internal parameters including the NN gains and output remain bounded⁽³⁰⁾. It should be noted that this particular control laws architecture is not

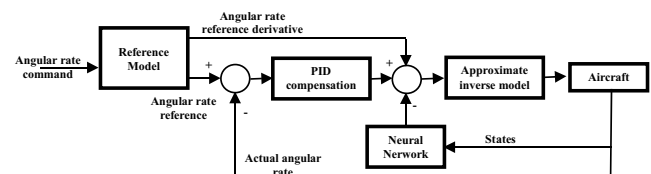


Figure 2. General scheme of the NLDI+NN control laws.

mandatory, in general, for the FDI scheme proposed in this paper. However, parameters computed within these control laws were determined to possess very good detection capabilities and were used as identifiers.

Consider the aircraft equations of motion in the general state variable form given by:

$$\begin{cases} \dot{\mathbf{x}}_1 = \mathbf{x}_2 \\ \dot{\mathbf{x}}_2 = f(\mathbf{x}, \mathbf{u}) \\ \dot{\mathbf{x}}_3 = g(\mathbf{x}, \mathbf{u}) \end{cases} \dots (1)$$

where $\mathbf{x} = \begin{bmatrix} \mathbf{x}_1 \\ \mathbf{x}_2 \\ \mathbf{x}_3 \end{bmatrix}$ is the state vector, \mathbf{u} is the control vector, and \mathbf{x}_2 is the vector of controlled variables. Let us define the pseudo-control as:

$$\mathbf{v} = \dot{\mathbf{x}}_2 = f(\mathbf{x}, \mathbf{u}) \dots (2)$$

Since, in general, f is non-invertible, an invertible approximation \hat{f} can be used to determine the controls \mathbf{u} necessary to achieve \mathbf{v} :

$$\mathbf{u} = \hat{f}^{-1}(\mathbf{x}, \mathbf{v}) \dots (3)$$

The error associated with the approximation is then expressed as:

$$\Delta = f(\mathbf{x}, \mathbf{u}) - \hat{f}(\mathbf{x}, \mathbf{u}) \dots (4)$$

With these notations, combining Equations (2) and (4), the system in Equation (1) can be re-written as:

$$\begin{cases} \dot{\mathbf{x}}_1 = \mathbf{x}_2 \\ \dot{\mathbf{x}}_2 = \Delta + \hat{f}(\mathbf{x}, \mathbf{u}) \end{cases} \dots (5)$$

Furthermore, let⁽³⁰⁾:

$$\hat{f}(\mathbf{x}, \mathbf{u}) = \mathbf{K}_i(\mathbf{x}_{1ref} - \mathbf{x}_1) + \mathbf{K}_p(\mathbf{x}_{2ref} - \mathbf{x}_2) + \mathbf{K}_d(\dot{\mathbf{x}}_{2ref} - \dot{\mathbf{x}}_2) + \dot{\mathbf{x}}_{2ref} - \mathbf{v}_{NN} \dots (6)$$

If the tracking error (TE) is defined as:

$$\begin{bmatrix} \mathbf{x}_{1ref} - \mathbf{x}_1 \\ \mathbf{x}_{2ref} - \mathbf{x}_2 \end{bmatrix} \dots (7)$$

then the error dynamics will result:

$$\dot{\mathbf{e}} = \begin{bmatrix} 0 & \mathbf{I} \\ -(\mathbf{K}_d + \mathbf{I})^{-1}\mathbf{K}_i & -(\mathbf{K}_d + \mathbf{I})^{-1}\mathbf{K}_p \end{bmatrix} \mathbf{e} + \begin{bmatrix} 0 \\ \mathbf{I} \end{bmatrix} (\mathbf{v}_{NN} - \Delta) \dots (8)$$

Next, the gain matrices \mathbf{K}_i , \mathbf{K}_p , and \mathbf{K}_d can be calculated with the goal of ensuring asymptotic stability of the error system.

For our specific case, let the controlled state variables be the roll, pitch, and yaw angular rates, that is $x_2 = [pqr]^T$. Within the NLDI control laws, longitudinal and lateral stick ($\delta_{lonstick}, \delta_{latstick}$) and pedal ($\delta_{dirpedal}$) displacements are first converted into angular rate commands:

$$\begin{aligned} p_{com} &= k_{lat} \delta_{latstick} \\ q_{com} &= \frac{g}{V} k_{lon} \delta_{lonstick} \\ r_{com} &= \frac{g}{V} (k_{dir} \delta_{dirpedal} + \text{Sin}(\phi)) \end{aligned} \dots (9)$$

Next, first and second order reference models are used to determine the desired aircraft response in terms of angular rates and their derivatives such that Level 1 handling qualities are ensured⁽³¹⁾ if tight command tracking is achieved. The reference models provide

filtered reference angular rates ($p_{ref}, q_{ref}, r_{ref}$) and reference angular accelerations ($\dot{p}_{ref}, \dot{q}_{ref}, \dot{r}_{ref}$) using first order roll rate and second order pitch and yaw rate transfer functions:

$$\begin{aligned} p_{ref}(s) &= \frac{1}{s + \tau_{roll}} p_{com}(s) \\ q_{ref}(s) &= \frac{\omega_{n_{pitch}}^2}{s^2 + 2\zeta_{pitch}\omega_{n_{pitch}} + \omega_{n_{pitch}}^2} q_{com}(s) \\ r_{ref}(s) &= \frac{\omega_{n_{yaw}}^2}{s^2 + 2\zeta_{yaw}\omega_{n_{yaw}} + \omega_{n_{yaw}}^2} r_{com}(s) \end{aligned} \dots (10)$$

The inputs to the dynamic inversion ($\dot{P}_c, \dot{q}_c, \dot{r}_c$) are computed using the expression:

$$\begin{bmatrix} \dot{p}_c \\ \dot{q}_c \\ \dot{r}_c \end{bmatrix} = \begin{bmatrix} U_p \\ U_q \\ U_r \end{bmatrix} - \begin{bmatrix} U_{pad} \\ U_{qad} \\ U_{rad} \end{bmatrix} \dots (11)$$

where ($U_{pad}, U_{qad}, U_{rad}$) are augmentation commands generated by adaptive NNs in order to compensate for the tracking errors e_p, e_q, e_r . These TEs are used to provide proportional, integral, and derivative compensation. Pseudo-controls in terms of angular acceleration commands (U_p, U_q, U_r) are evaluated using:

$$\begin{aligned} U_p &= \left(K_{p_p} + \frac{K_{i_p}}{s} + K_{d_p} s \right) e_p + s.p_{ref} \\ U_q &= \left(K_{p_q} + \frac{K_{i_q}}{s} + K_{d_q} s \right) e_q + s.q_{ref} \\ U_r &= \left(K_{p_r} + \frac{K_{i_r}}{s} + K_{d_r} s \right) e_r + s.r_{ref} \end{aligned} \dots (12)$$

where K_p, K_i , and K_d are the constants of a proportional-integral-derivative type controller, respectively. These gains are determined to achieve adequate stability and performance characteristics at closed loop conditions with the assumption that the inversion is perfect or, equivalently, the NN compensation is perfect. Dynamic inversion is then used to determine the necessary control surface deflections ($\delta_a, \delta_e, \delta_r$). Initially, control surface commands ($\delta_{a_{com}}, \delta_{e_{com}}, \delta_{r_{com}}$) are obtained with the following equation:

$$\begin{bmatrix} \delta_{a_{com}} \\ \delta_{e_{com}} \\ \delta_{r_{com}} \end{bmatrix} = \mathbf{B}^{-1} \begin{bmatrix} \dot{p}_c - L_1 \\ \dot{q}_c - M_1 \\ \dot{r}_c - N_1 \end{bmatrix} \dots (13)$$

L_1, M_1 , and N_1 are the non-linear terms of the moment equations and \mathbf{B} is the state space system control matrix computed at one particular flight condition. Finally, the control surface actual deflections are computed from $\delta_{a_{com}}, \delta_{e_{com}}, \delta_{r_{com}}$ according to a control allocation algorithm.

An improved Radial Basis Function (RBF) NN to produce the compensation terms U_{pad}, U_{qad} and U_{rad} in Equation (11) has been implemented for the purpose of this paper: the Extended Minimal Resource Allocation Network⁽³²⁾ (EMRAN). The EMRAN features a growing and pruning mechanism allowing the allocation of additional neurons in regions of the state space where the mapping accuracy is poor while avoiding the excessive growth of the network. Only the parameters of the most activated neurons are updated; therefore, the computational effort is minimised for this class of neural augmentation. For Gaussian basis functions, the estimate is computed with the expression:

$$\hat{y}(\mathbf{x}, \theta) = \sum_{i=1}^M w_i e^{-\frac{(x - \mu_i)^2}{2\sigma_i^2}} \dots (14)$$

where x is the input vector, θ is the set of parameters to be tuned by the learning algorithm including the weight w , the Gaussian centre positions μ , and the variances σ . A new neuron is initiated if three distinct criteria are simultaneously satisfied: the estimation error, the windowed estimation error, and the distance from the input to the nearest centre must each be larger than selected thresholds. If one of the criteria is not met, the tuning parameters are updated using the relationship:

$$\theta(k+1) = \theta(k) - \eta \left. \frac{\partial \hat{y}(k)}{\partial \theta(k)} \right|_{(k)} \cdot e(k) \quad \dots (15)$$

where $e(k)$ is the estimation error and η is the learning rate.

3.3 Flight simulator experiment

The experimental data were generated in the WVU 6 degrees-of-freedom (DOF) motion-based flight simulator. The Motus 600 Flight Simulator was interfaced with an external computer on which the customised WVU IFCS F-15 research aircraft model was run within the Matlab/Simulink environment to drive the entire simulator system. This offers a very realistic flight simulation environment allowing ‘true’ motion cues and high quality visual cues.

To define the self as completely and accurately as possible, adequate coverage of the state space must be achieved. Extensive experimental flight data is necessary to provide sufficient information to ‘train’ the AIS system by generating antibodies capable to recognise between normal and abnormal situations with high rate of success. Different flight scenarios were performed over a wide area of the flight envelope, defined based on nine specific reference points (see Fig. 3) for Mach numbers between 0.6 and 0.9 and altitudes between 9,000ft and 31,000ft. Flight tests start at steady state flight condition #1 and continue to cover the nine points as described by the arrows in Fig. 3. For example, one flight test starts at #1, the aircraft is accelerated at constant altitude to point #4, descended at constant speed to point #5, and then returned to point #4 and #1. A total of eight such tests are necessary to cover the testing flight envelope. The data from these tests are used to develop the failure detection and identification scheme. Additional tests at intermediate points (A, B, C, and D in Fig. 3) were performed to be used as validation data.

The set of flight scenarios, lasting between 10 and 20 minutes each, were designed to include steady state flight conditions, transitions between steady state conditions, and mild to moderate manoeuvres such as doublets, co-ordinated turns, and turns at progressive bank angles. These flight tests were first performed under normal flight conditions. Then, they were repeated under

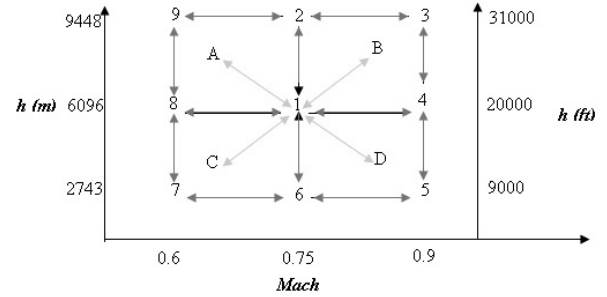


Figure 3. Testing flight envelope.

various failure scenarios considering only one failure at a time, for development and testing purposes. Additional test data were also collected to be used for validation. The data from the simulator were acquired at a rate of 50Hz. The simulated failures tested for the purpose of this paper are outlined in Table 1.

4.0 DESIGN OF THE AIS FOR FDI SCHEME DEVELOPMENT

4.1 Definition of self-characterising variables

A critical element for the success of the AIS-based FDI scheme is the selection of the appropriate parameters (features) to capture the dynamic signature of each and every type of failure. These parameters characterise the ‘self’ – or normal conditions and – for that matter – the ‘non-self’, or the abnormal conditions. The candidate parameters for self/non-self definition can, in general, be grouped in the following five categories⁽²¹⁾: aircraft state variables, pilot input variables, stability and control derivatives, variables generated within the control laws, and derived variables. They can be instantaneous samples or time histories over constant or variable windows. After a preliminary analysis⁽³³⁾ of the detection potential of a large number of candidate features, the following parameters were selected for further use within the FDI scheme:

- angular rate tracking errors on all three channels x_{TE} :

$$x_{TE} = x - x_{ref} \quad \dots (16)$$

Table 1 Simulated failures

Failure Category	Failure Type	Description
Actuator	Stabilator	Blockage of the left or right stabilator at 8deg and 2deg
	Aileron	Blockage of the left or right aileron at 8deg and 2.5deg
	Rudder	Blockage of the left or right rudder at 8deg and 4deg
Sensor	Large Step Bias (LSB)	Step bias of 10 deg/s and 5 deg/s in the roll and pitch rate sensors and 3 deg/s and 1 deg/sec in the yaw rate sensor
	Large Fast Drifting Bias (LFDB)	
Structural	Wing damage to produce loss of aerodynamic properties and mass	Loss of 15% of the left or right wing, affecting the ‘efficiency’ of the aileron control surface. Loss of 6% of the left or right wing without affecting the ‘efficiency’ of the aileron control surface.
Engine	Loss of power/thrust	Loss of 98% and 60% of the thrust of the left or right engine.

where $x = p, q, \text{ or } r$ (roll, pitch, or yaw rate) and x_{ref} is the reference rate determined within the model-following control laws directly from pilot input to meet first or second order responses as required for good handling qualities.

- selected aircraft states such as sideslip angle (β) and longitudinal acceleration (a_x).
- NN output on all three channels (angular accelerations)

$$NN_{out} = [NN_{outp}, NN_{outq}, NN_{outr}] = [U_{pads}, U_{qads}, U_{rad}] \dots (17)$$

- Main quadratic estimation error (MQEE) parameter^(13,16):

$$MQEE(k) = \frac{1}{2} \left[(p(k) - \hat{p}_{MNN}(k))^2 + (q(k) - \hat{q}_{MNN}(k))^2 + (r(k) - \hat{r}_{MNN}(k))^2 \right] \dots (18)$$

where $p(k), q(k), \text{ and } r(k)$ are measurements of angular rates at sample k and $\hat{p}_{MNN}(k), \hat{q}_{MNN}(k), \hat{r}_{MNN}(k)$ and are neural estimates of the angular rates based on sensor measurements including the respective gyro, over a specified time window.

- Output quadratic estimation error (OQEE) parameter^(3,16):

$$OQEE(k) = \frac{1}{2} \left[(\hat{p}_{DNN}(k) - \hat{p}_{MNN}(k))^2 + (\hat{q}_{DNN}(k) - \hat{q}_{MNN}(k))^2 + (\hat{r}_{DNN}(k) - \hat{r}_{MNN}(k))^2 \right] \dots (19)$$

where $\hat{p}_{DNN}(k), \hat{q}_{DNN}(k), \text{ and } \hat{r}_{DNN}(k)$ are neural estimates of the angular rates based on sensor measurements that do NOT include the respective gyro, over a specified time window.

- Decentralised quadratic estimation error (DQEE) parameter^(13,16):

$$DQEE_x(k) = \frac{1}{2} (\hat{x}_{DNN}(k) - x(k))^2, \quad x = p, q, r \dots (20)$$

The parameters defined in Equations (16) through (20) were grouped in five feature configurations for self definition, as presented in Table 2. Self#1 includes the NN outputs in terms of roll, pitch, and yaw rates. Self#2 considers additionally the *DQEE* parameter for the three angular accelerations. Self#3 consists of the NN outputs and the angular rate tracking errors on the three channels. Self#4 is the same as Self#2 plus the *MQEE* and *OQEE* parameters for the roll, pitch and yaw rate channels. Since the Self#2, #3, and #4 contain parameters that are based on NN estimations of sensor outputs, it is expected that these configurations capture the malfunction of the sensors. Finally, Self#5 includes the NN output of the yaw gyro channel, the sideslip angle, and the longitudinal acceleration of the aircraft.

Table 2
Feature configurations for self definition

Self Number	Features	Solution Space Dimension
Self#1	NN_{outx}	3
Self#2	NN_{outx} and $DQEE_x$	6
Self#3	NN_{outx} and x_{TE}	6
Self#4	$NN_{outx}, MQEE, OQEE$ and $DQEE_x$	8
Self#5	NN_{outr}, β and a_x	3

4.2 Representation of self

A process that is of absolute importance for the AIS is the matching between the detectors and the explored data (data subject to the detection process). This is the equivalent of the biological matching

between the antibodies and antigens, which is the basis for the recognition and selective elimination mechanism of intruding agents. In general, the matching rules rely on metrics for comparison and a logic to produce a binary output – match or not-match. They depend on the type of data representation. Data representation has an important impact on algorithm effectiveness and performance. It determines the possible matching rules, the detector generation mechanisms, and the detection process. In this paper, a real-valued vector representation is implemented. Within the real-valued vector representation, each data item is a vector of real numbers⁽³⁴⁾. The matching rules and the measure of difference or similarity are based on the numeric elements of the vector, which are implicit in the Euclidian distance between the components tested⁽³⁵⁾. With this type of representation, a condensed data version using a reduced number of parameters can be achieved by replacing clusters of data by circumscribed geometrical hyper-bodies. The characteristics (shape) of these bodies have an impact on the efficiency of the detector generation process and on the detection itself. They determine how well the non-self is covered, how many detectors are necessary, and how intensive the computational process is. For the purpose of this paper, only hyper-sphere shapes for the self/non-self are considered.

4.3 Generation of detectors

Existing algorithms have been evaluated, customised, and integrated within an evolutionary algorithm (EA)-based design tool for detector generation and optimisation⁽³⁶⁾. The two-phase EA achieves optimisation of the detector set for good detection performance and computational effectiveness. However, for the purpose of this paper only the first phase was considered. An enhanced negative selection algorithm for real-valued representation with variable detector radius (ENSA-RV) has been designed and implemented.

Starting with an initial set of candidate detectors, located randomly in the non-self of an n -dimensional hyper-space, the algorithm performs a selection process based on two criteria: no overlapping with the self and a desired predetermined coverage of the non-self. At every iteration, the radius of each detector is computed using the distance between the candidate detector and the nearest self cluster. Since a minimum radius r_m is permitted for detectors, the distance between centres must be greater than or equal to the sum of r_m and the radius of the cluster r_c . Because a better coverage is achieved when a minimum overlapping among detectors is allowed, an overlapping measure w_i of a detector with respect to the others is calculated during the maturation process⁽²⁰⁾. For an overlapping threshold value w_{thr} , every detector is selected as mature if the condition $w_i \leq w_{thr}$ is satisfied. Eventually, if $w_i = 0$, that particular detector is selected to have a number of $N_{clon} = 2n$ clones around it. The centre of the first clone is placed at a distance equal to one radius and along a random direction. The remaining clone centres are generated at 90° angles with respect to the first one in $n-1$ orthogonal planes. If $0 < w_i \leq w_{thr}$, only one centre clone is generated at a direction opposite to the nearest element (mature detector or cluster self). For this operation, an updating rule is used to determine how far the clone element is located at every iteration. Additionally, the *NMOV* smallest rejected detectors are selected to be moved in opposite direction of the mean centre of the k -nearest elements. The same updating rule used in the detector cloning operation is used in the detector movement step as well. Finally, a set of *NRD* random centres is inserted; the radius of the mature detectors calculated, and the coverage and overlapping computed. The process can be stopped after a prescribed number of iterations, when a prescribed maximum number of acceptable detectors has been reached, or when a desired coverage of the non-self has been achieved. The algorithm can optimise the requirements for no overlapping among non-self detectors and self and minimum un-covered areas in the non-self.

The five sets of features presented in Table 2 were used to define the ‘self’ as a set of hyper-spherical clusters. Corresponding detectors were generated in each case.

5.0 IMMUNITY-BASED DETECTION AND IDENTIFICATION SCHEME

5.1 Integration of self patterns

The capabilities of the four different sets of features for the detection of every type of failure have been analysed. The quantitative evaluation has been defined by using two specific metrics. Assuming typical binary outcomes, the results of the detection can be categorised as:

- TP – True Positives: abnormal data points detected as abnormal
- TN – True Negatives: normal data points not detected as abnormal
- FP – False Positives: normal data points detected as abnormal
- FN – False Negatives: abnormal data points not detected as abnormal

The detection rate (*DR*) is defined as the ratio between abnormal data points detected as abnormal divided by the total amount of abnormal data points:

$$DR = \frac{TP}{TP + FN} \times 100 \quad \dots (21)$$

The false alarm rate (*FA*) is defined as the ratio between normal data points detected as abnormal divided by the total amount of normal data points:

$$FA = \frac{FP}{TN + FP} \times 100 \quad \dots (22)$$

The detection performance for every self and failure has been determined and is presented in Table 3 in terms of detection rate for high magnitude failures and false alarms. The results represent the averages over different tests around the flight envelope. Note that every self presents at least one acceptable performance for one of the failures considered. For instance, the Self#1 shows a poor detection for the sensor, aileron, and engine failures, but an acceptable detection for all other failures with very low false alarms. The fact that different selves favour the detection of particular types of failures is used in this paper to develop an integrated scheme where different self configurations ensure overall high detection rate and low number of false alarms.

5.2 Detection and identification scheme using a hierarchical multi-self strategy

The Hierarchical Multi-Self (HMS) strategy scheme relies on the assumption that within a class of failures, differences between failed elements may be captured by different numbers and/or types of ‘features’ as compared to the ones necessary to detect the class. Thus, a specific set of parameters could favour the identification of some particular failures better than others. The method avoids using one large dimensional self for centralised detection and/or identification and instead divides the process into several components, each supported by lower dimensional selves. This approach requires building failure specific ‘selves’ and identification of low dimensional spaces for hierarchical ‘selves’ definitions. As shown in Fig. 4, the online detection and identification process is performed using two main components. The first one uses an integrated block of self patterns which performs the detection phase. The second component, where the identification phase is performed, attempts to ensure the correct identification of categories and sub-categories of failures at different levels.

Detection is considered to be the process leading to declaring that an abnormal condition in any of the sub-systems is present. During

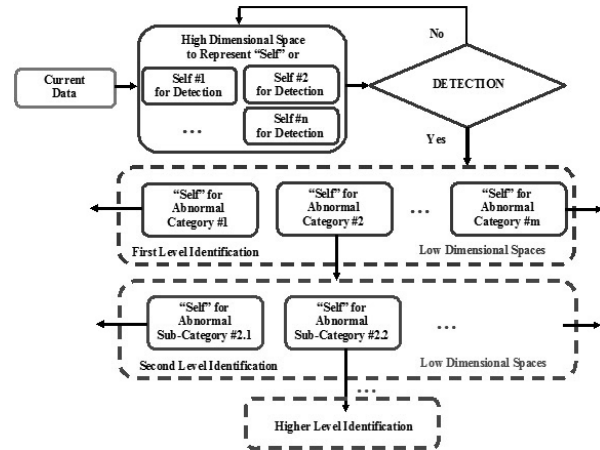


Figure 4. Hierarchical multi-self strategy for online failure detection and identification.

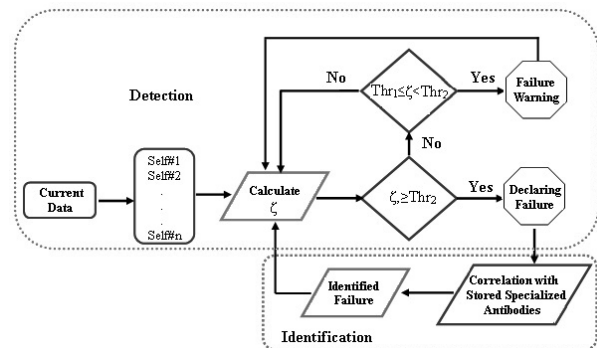


Figure 5. Block diagram of the proposed HMS strategy for online failure detection and identification.

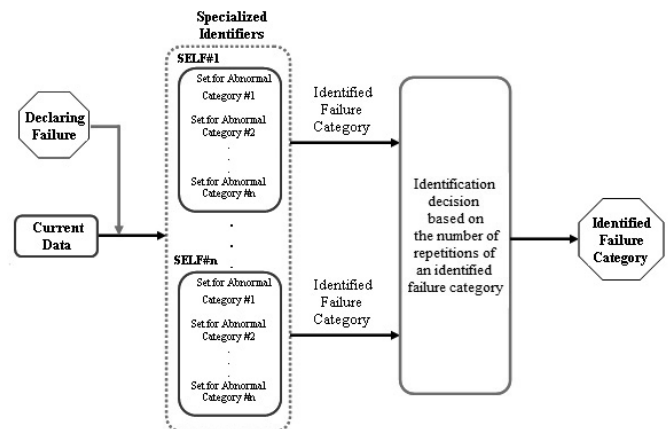


Figure 6. Block diagram of the identification phase of proposed HMS strategy.

this phase, sets of current values of the features measured in flight at a certain sampling rate are compared against the detectors that have been generated for every self configuration as shown in Fig. 5. A detection parameter ζ is calculated, which represents the number of consecutive points over a window ω that trigger detectors, summed over all selves. If ζ is within a certain range, a failure warning is issued, but if ζ exceeds an upper bound, a failure is declared and the identification phase starts.

Table 3
Detection performance of different self configurations

Self Configuration	# detectors	Failure Test Data Detection Rates (%)							Nominal Test Data False Alarms (%)
		Actuator Failure			Sensor Failure		Structural Failure	Engine Failure	New data
		Stabilator	Aileron	Rudder	LSB	LFDB			
SELF#1	875	L: 99-96 R: 98-97	L: 99-96 R: 99-96	L: 93-01 R: 88-76	p: 19-52 q: 15-37 r: 53-92	p: 24-67 q: 15-67 r: 62-48	L: 99-80 R: 99-98	L: 33-13 R: 33-22	1-A: 0-60 1-B: 1-17 1-C: 0-93 1-D: 1-05
SELF#2	1331	L: 99-98 R: 99-98	L: 99-96 R: 100	L: 96-14 R: 88-41	p: 92-47 q: 95-32 r: 93-77	p: 84-03 q: 78-07 r: 95-58	L: 99-86 R: 99-74	L: 32-12 R: 40-06	1-A: 2-13 1-B: 1-25 1-C: 0-08 1-D: 0-96
SELF#3	325	L: 98-62 R: 100	L: 99-98 R: 99-97	L: 62-59 R: 43-85	p: 9-51 q: 98-98 r: 89-76	p: 2-60 q: 99-57 r: 91-00	L: 100 R: 100	L: 15-10 R: 7-71	1-A: 0 1-B: 0-01 1-C: 0 1-D: 0
SELF#4	918	L: 92-97 R: 99-30	L: 99-98 R: 100	L: 74-90 R: 53-00	p: 95-72 q: 66-36 r: 94-84	p: 97-82 q: 58-99 r: 97-88	L: 98-92 R: 100	L: 24-44 R: 15-36	1-A: 0-61 1-B: 1-24 1-C: 0-22 1-D: 1-30
SELF#5	512	L: 90-66 R: 56-94	L: 0-83 R: 4-17	L: 66-43 R: 69-39	p: 2-40 q: 1-61 r: 31-75	p: 0-66 q: 0-18 r: 31-75	L: 39-59 R: 51-15	L: 17-19 R: 25-25	1-A: 0-74 1-B: 0-01 1-C: 1-14 1-D: 0-04

Table 4
Detection performance of the HMS strategy

Failure Test Data Detection Rates (%) (Convention: x-x = Magnitude – Subsystem fail)							Nominal Test Data False Alarms (%)
Actuator Failure			Sensor Failure		Structural Failure	Engine Failure	New data
Stabilator	Aileron	Rudder	LSB	LFDB			
2-L: 99-8 8-L: 100 2-R: 100 8-R: 100	2-L: 95-6 5-L: 100 8-L: 100 2-R: 93-5 8-R: 100	4-L: 91-4 8-L: 99-2 4-R: 85-9 8-R: 97-7	5-p: 95-4 10-p: 97-1 5-q: 99-8 10-q: 100 3-r: 100	10-p: 97-6 10-q: 100 1-r: 97-3 3-r: 100	6-L: 99-3 15-L: 100 6-R: 99-8 15-R: 100	60-L: 36-16 98-L: 62-75 60-R: 16-07 98-R: 60-71	1-A: 2-08 1-B: 1-92 1-C: 1-57 1-D: 1-59

Table 5
Pre-Identification performance of the HMS strategy

Failure Type	Failure Category (Identification Rates (%))						
	Stabilator	Aileron	Rudder	Sensor	Structural	Engine	Unknown
2deg-L: Stabilator	98·16	0	0	0	0	0	3·41
8deg-L: Stabilator	96·58	0	0	0·09	0	0	1·73
2deg-R: Stabilator	96·41	0	0	0	0	0	2·30
8deg-R: Stabilator	97·69	0	0	2·26	0·98	0	0·34
2·5deg-L: Aileron	0·32	99·10	0	0·02	0·53	0·02	0
8deg-L: Aileron	0·83	96·29	0	0·07	2·8	0	0
2·5deg-R: Aileron	0	98·37	0	0·24	1·25	0·12	0
8deg-R: Aileron	0	100	0	0	0	0	0
4deg-L: Rudder	0	4·85	92·83	2·23	0·07	0	0
8deg-L: Rudder	0	0·09	91·03	8·85	0·008	0	0
4deg-R: Rudder	0	0·62	98·05	1·26	0·04	0	0
8deg-R: Rudder	0	0·47	98·61	0·9	0	0	0
5-p: LSB	0	0·41	0	94·74	0·14	4·32	0·37
10-p: LSB	0	0·33	0	95·76	0·08	1·26	2·55
5-q: LSB	1·36	0	0	97·56	0	1·07	0
10-q: LSB	0	0	0	100	0	0	0
1-r: LSB	0·04	1·45	0	94·35	0·39	3·33	0·41
3-r: LSB	0	0	0	99·66	0	0·33	0
6-L: Structural	0	3·03	0	0·10	96·83	0	0·02
15-L: Structural	1·15	3·25	0	0	94·21	0	1·37
6-R: Structural	0·15	1·93	0	0	97·79	0	0·10
15-R: Structural	0·07	2·29	0	0	96·91	0	0·70
60%-L: Engine	0	8	0	1	6·16	84·83	0
100%-L: Engine	0	0·71	0	4·03	0·32	94·92	0
60%-R: Engine	0	21·66	0	0·45	6·06	71·81	0
100%-R: Engine	0	1·77	0	4·23	0·15	93·83	0

Within the non-self detectors, sub-sets can be identified to correspond to specific categories of abnormal conditions for identification purposes. The approach implies the use of the negative selection strategy and a *priori* knowledge of specialised detectors⁽²¹⁾. However, positive selection can also be applied to determine the sets of specialised detectors or identifiers for known failures for which data is available. Such information can be obtained from tests, simulation, or analysis. Thus, the identification phase of the HMS is based on identifiers instead of detectors. This implies that it is not necessary to use for identification the same antibodies used in the detection phase (called detectors). For detection, the detectors are designed with a variable size in such a way that they cover the largest volumes of the non-self space as possible. The bigger the detectors are, the smaller the detection time. However, bigger detectors may not be convenient during the identification phase, since they can be activated for two or more types of failure, so they need to be redefined using a finer resolution. The process of selecting the identifiers is performed by applying the positive selection method to the flight tests at failure conditions. In this way, the candidate identifiers are labeled according to the type of failure and will be selected as identifiers when the activation is guaranteed only for that particular failure. With this approach, the number of false identifications is reduced considerably.

The identification phase is performed in two steps:

- *Pre-identification.* The failure is attributed to one of the four categories: control surface, sensor, structural, or engine failure. As shown in Fig. 6, the category is determined based on the number of times each set of identifiers is activated for a particular failure category. The preliminary result is compared with the output of the other identifier sets. The most repetitive result will be considered as the identified category.
- *Identification.* If the failure is classified as actuator failure, the failure is identified to be a left or right stabilator, aileron, or rudder failure. If pre-identified as a sensor failure, it is identified to be a roll, pitch, or yaw rate sensor failure. If pre-identified as a structural failure, the abnormal condition may be identified as affecting the left or right wing. Finally, if a propulsion failure was declared, it must now be determined if it affects the left or the right engine. The identification is performed by analysing which of the identifiers have been activated. The identifiers have been labeled previously to represent specific sub-categories of failures through an off-line process based on positive selection strategy performed repeatedly on selves at each failure sub-category. The identification decision is taken based on a majority vote.

To test the detection and identification capabilities of the proposed HMS strategy, the five selves outlined in Table 3 have been combined in an integrated scheme as described in Fig. 5. The results are presented and analysed in the next section.

6.0 TEST RESULTS, ANALYSIS, AND EVALUATION OF THE FDI SCHEME PERFORMANCE

6.1 Detection performance of the HMS strategy

The detection outcome is a binary output produced at the sampling rate of 50Hz based on a moving time window of width $\omega = 10$ seconds for each self and a relative detection threshold of 30%, which represents the number of consecutive points over the window that trigger detectors, summed over all selves. With these parameters, the detection time for all cases considered was less or equal to 0.06s. The results are summarised in Table 4 for different magnitudes of failures and represent the average over different points in the flight envelope.

As compared to the results presented in Table 3 for individual/isolated detector sets, the HMS approach improves significantly the detection performance for all type of failures. For the stabilator, aileron, yaw gyro, and structural failures, for example, the detection rate reaches 100%. Not only the detection rate is improved; the false alarms are also reduced significantly.

Note that the engine failure is the only one that presents a lower detection rate. In fact, none of the five selves outlined in the Table 3 achieves a very good detection performance for this type of failure. This is due to the fact that the available identifiers possibly relevant to engine operation such as sideslip angle and longitudinal acceleration included in self #5 are not sufficient to capture the signature of this failure and additional measurements of engine internal parameters must be used. A more detailed engine model providing such information was not available for the purpose of this paper.

As shown in the results, the good detection performance of the HMS is recorded over a wide area of the flight envelope. Note that validation data includes flight tests to the points A, B, C, and D as shown in Fig. 4. The low number of false alarms recorded implies that the nine points selected to define the testing area of the flight envelope are sufficient and no additional test at intermediate points are necessary to train the AIS.

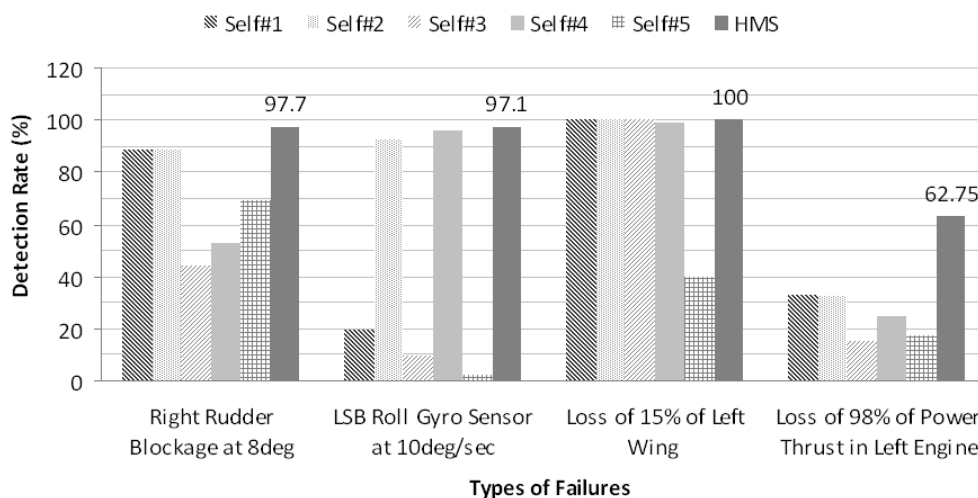


Figure 7. Detection rate of different self definitions compared with the proposed HMS strategy.

Table 6
Identification Performance of the HMS strategy

a. Actuator Sub-System Failures

Failure Type	L:	R:	L:	R:
	Stabilator	Stabilator	Aileron	Aileron
2deg-L: Stabilator	100	0	--	--
8deg-L: Stabilator	100	0	--	--
2deg-R: Stabilator	0	100	--	--
8deg-R: Stabilator	0	100	--	--
2·5deg-L: Aileron	--	--	100	0
8deg-L: Aileron	--	--	100	0
2·5deg-R: Aileron	--	--	0	100
8deg-R: Aileron	--	--	0	100

b. Sensor Sub-System Failures

Failure Type	p: LSB	q: LSB	r: LSB
5deg/sec-p: LSB	100	0	0
10deg/sec-p: LSB	100	0	0
5deg/sec-q: LSB	2·03	97·97	0
10deg/sec-q: LSB	1·6	98·40	0
1deg/sec -r: LSB	0	0	100
3deg/sec -r: LSB	0	0	100

c. Structural Sub-System Failures

Failure Type	L: Structural	R: Structural
6%-L: Structural	100	0
15%-L: Structural	100	0
6%-R: Structural	0	100
15%-R: Structural	0	100

d. Engine Sub-System Failures

	L: Engine	R: Engine
60%-L: Engine	100	0
100%-L: Engine	98·75	1·25
60%-R: Engine	0	100
100%-R: Engine	0	100

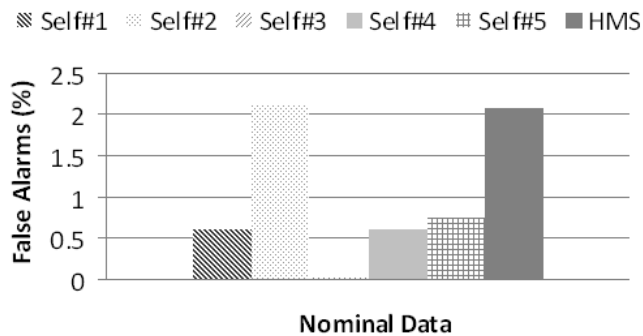


Figure 8. False alarms of different self definitions compared with the proposed HMS strategy.

In general, these results confirm the fact that better detection performance can be achieved by using an integrated self scheme instead of considering individual self configurations.

6.2 Identification performance of the HMS strategy

Once a failure condition is declared by the detection phase scheme, the identification phase starts to perform a pre-classification according to the four category failures considered. Tables 5 and 6 summarise the results for the identification of different types of failures using a new set of flight validation data different from the one used for training. Note that unknown abnormal conditions have been considered as well. This unknown condition is declared when some antibodies are activated but they do not belong to any of the identifiers set. It should be noticed that the rudder failure was considered only during the pre-identification process. This is because the effect of this type of failure on the dynamics of the aircraft is practically invariant with the component failed, left or right. Therefore, the accommodation tasks related to this failure can be considered the same for either of the two sides. This makes the actual identification of this type of failure irrelevant.

These results show excellent failure pre-identification and identification achieved using the HMS strategy. Figures 7 through 9 summarise the main results in terms of detection and pre-identification performance for some types of failures. Figure 7 presents a comparison between the selves outlined in Table 2 and the HMS scheme for high magnitude failures. Note that the HMS achieves high detection rate for all failure cases while keeping low false alarms, as shown in Fig. 8. The use of HMS provides potential benefits as an alternative to individual 'self' configurations. In addition, Fig. 9 shows that the HMS is capable of high identification performance for a variety of failure categories.

Although the performance results of the HMS have been obtained using a hyper-sphere self/non-self representation, the approach can be expanded to other hyper-shapes such as hyper-cubes, hyper-ellipse, or even the combination of them. Thus, the HMS can produce a flexible scheme and extract the best characteristics of different feature definitions and integrate them to improve detection performance characteristics.

In this paper, all the variables used to create the selves are defined in the time domain. It is expected that including frequency domain identifiers could improve the access to the fingerprints of certain failure classes. The HMS would permit the development of such hybrid detector spaces within the same scheme.

All the analysis presented in this paper is based on data generated from flight simulation tests. However, the authors have performed preliminary tests of a similar FDI scheme using actual flight data from a reduced-size unmanned aeroplane⁽³⁷⁾, which confirmed the promising capabilities of the proposed approach. The on-line computational effort is reduced allowing for real-time operation without special algorithms or equipment. It is envisioned that the AIS paradigm in combination with the HMS can successfully be used for

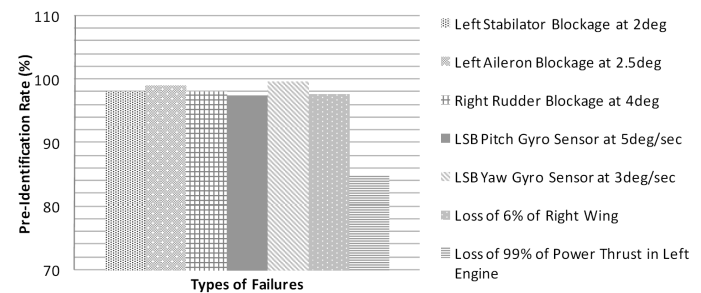


Figure 9. Pre-identification performance of the proposed HMS strategy.

numerous real-time aerospace applications such as providing increased situational awareness for pilots, control, or monitoring systems, aircraft system health management, augmentation of adaptive flight control laws, and monitoring and control of space exploration systems.

7.0 CONCLUSIONS

An integrated artificial immune system-based scheme for the detection and identification of aircraft sub-system failures has been developed and implemented using a novel hierarchical multi-self strategy. Testing on a 6-DOF motion-based flight simulator for a wide region of the flight envelope demonstrated the effectiveness of the HMS for aircraft FDI.

Based on the observation that reduced size sets of specific identifiers can typically capture the fingerprint of numerous individual/isolated failures, the implementation of the HMS allows consistent and comprehensive integration and substantial flexibility for easy expansion and updating when additional information becomes available.

The detection and identification capabilities have been demonstrated in terms of low false alarm and high detection and identification rates for different aircraft actuator, sensor, propulsion, and structure failures/damages. The results confirm the fact that using an integrated multiple-self approach instead of considering self configurations separately can significantly improve the detection performance while ensuring that the multi-dimensionality of the feature space remains manageable.

The results presented in this paper demonstrate that the proposed HMS within the AIS paradigm for aircraft FDI is able to mitigate multi-dimensionality issues, distinguish between numerous types of failure, and achieve robustness with respect to failure severity and difference in flight conditions over large regions of the flight envelope.

The proposed approach can potentially have a significant impact in the areas of failure detection and adaptive flight control systems by providing the tools for a comprehensive/integrated solution to the problem of aircraft sub-system FDI.

Recommendations for future work include the development of hybrid identifier sets (in the time domain and frequency domain), the investigation of robustness with actual flight data, and the analysis of the interaction with the human pilot.

ACKNOWLEDGMENTS

This research effort was sponsored by NASA Aviation Safety Program through a grant within the Integrated Resilient Aircraft Control project. Special thanks to the volunteer pilots Alejandro Posada, Steven Mullins, Steven Hard, and Ondrej Karas for performing the tests in the flight simulator.

REFERENCES

1. TOTAH, J., KRISHNAKUMAR, K. and VIKEN, S. Stability, maneuverability, and safe landing in the presence of adverse conditions, Integrated Resilient Aircraft Control Technical Plan, Aviation Safety Program, Aeronautics Research Mission Directorate, NASA, 2007, http://www.aeronautics.nasa.gov/nra_pdf/irac_tech_plan_c1.pdf
2. SRIVASTAVA, A.N., MAH, R.W. and MEYER, C. Automated detection, diagnosis, prognosis to enable mitigation of adverse events during flight, Integrated Vehicle Health Management Technical Plan, Aviation Safety Program, Aeronautics Research Mission Directorate, NASA, 2008, http://www.aeronautics.nasa.gov/nra_pdf/ivhm_tech_plan_c1.pdf
3. YOUNG, S.D. and QUON, L. Integrated intelligent flight deck, Integrated Intelligent Flight Deck Technical Plan, Aviation Safety Program, Aeronautics Research Mission Directorate, NASA, 2007, http://www.aeronautics.nasa.gov/nra_pdf/iifd_tech_plan_c1.pdf
4. YOUNG, R. and ROHN, D. Aircraft aging and durability project, Aircraft Aging and Durability Project Technical Plan, Aviation Safety Program, Aeronautics Research Mission Directorate, NASA, 2007, http://www.aeronautics.nasa.gov/nra_pdf/aad_tech_plan_c1.pdf
5. WHITE, J. NASA's Aviation Safety Program, 44th Annual AIAA Aerospace Sciences Meeting, Reno, Nevada, USA, January 2006.
6. WILSKY, A.S. Failure detection in dynamic systems, Agard LS-109, Neuilly Sur Seine, France, October 1980, 2.1-2.14.
7. MARCOS, A., GANGULI, S. and BALAS, G. Application of fault detection and isolation to a Boeing 747-100/200 aircraft, Proceedings of the AIAA Guidance, Navigation and Control Conference, AIAA Paper 02-4944, Monterey, CA, USA, August 2002.
8. SHIN, J.Y., WU, N.E. and BELCASTRO, C. Linear parameter varying control synthesis for actuator failure, based on estimated parameter, Proceedings of the AIAA Guidance, Navigation and Control Conference, AIAA Paper 02-4546, Monterey, CA, USA, August 2002.
9. NARENDRA K.S. and BALAKRISHNAN J. Adaptive control using multiple models, IEEE Transactions on Automatic Control, 1997, **42**, (2), pp 171-187.
10. NAPOLITANO, M.R., CASDORPH, V., NEPPACH, C. and NAYLOR, S. Online learning neural architectures and cross-correlation analysis for actuator failure detection and identification, *Int J Control*, 1996, **63**, (3), pp 433-455.
11. JAKUBEK, S. and STRASSER, T. Fault diagnosis using neural networks with ellipsoidal basis functions, Proceedings of the American Control Conference, Anchorage, AK, USA, 2002, pp 3846-3851.
12. LOU S.J., BUDMAN H. and DUEVER T.A. Comparison of fault detection techniques: problem and solution, Proceedings of the American Control Conference, Anchorage, AK, USA, 2002, pp 4513-4518.
13. NAPOLITANO, M.R., YOUNGHAWN, A. and SEANOR, B. A fault tolerant flight control system for sensor and actuator failures using neural networks, *Aircraft Design*, 2000, **3**, (2).
14. IVERSON, D. Inductive system health monitoring, Proceedings of the 2004 International Conference on Artificial Intelligence (IC-AI'04), Las Vegas, NV, USA, 2004, pp 605-611.
15. NAPOLITANO, M.R., NEPPACH, C.D., CASDORPH, V., NAYLOR, S., INNOCENTI, M. and SILVESTRI, G. A neural-network-based scheme for sensor failure detection, identification, and accommodation, *AIAA J Guidance, Control, and Dynamics*, 1995, **18**, (6), pp 1280-1286.
16. PERHINSCHI, M.G., NAPOLITANO, M.R., CAMPA, G. and FRAVOLINI, M.L. Integration of fault tolerant system for sensor and actuator failures within the WVU NASA F-15 simulator, AIAA Guidance, Navigation, and Control Conference, Austin, TX, USA, August 2003.
17. NGUYEN, N., KRISHNAKUMAR, K., KANESHIGE, J. and NESPECA, P. Dynamics and adaptive control for stability recovery of damaged asymmetric aircraft, Proceeding of the AIAA Guidance, Navigation, and Control Conference and Exhibit, Keystone, Colorado, USA, August 2006.
18. TESSLER, A. Structural analysis methods for structural health management of future aerospace vehicles, NASA/TM-2007-214871, Langley Research Center, Hampton, Virginia, USA, 2007.
19. KRISHNAKUMAR, K. Artificial immune system approaches for aerospace applications, AIAA-2003-0457, Proceeding of the 41st Aerospace Sciences Meeting & Exhibit, Reno, Nevada, USA, 2003.
20. DASGUPTA, D., KRISHNAKUMAR, K., WONG, D. and BERRY, M. Negative selection algorithm for aircraft fault detection, G. Nicosia *et al* (Eds.): ICARIS 2004, LNCS 3239, pp. 1-13.
21. PERHINSCHI, M.G., MONCAYO, H. and DAVIS, J. Integrated framework for aircraft sub-system failure detection, identification, and evaluation based on the artificial immune system paradigm, Proceeding of the AIAA Guidance, Navigation, and Control Conference, Chicago, IL, USA, August 2009.
22. PERHINSCHI, M.G., NAPOLITANO, M.R., CAMPA, G. and FRAVOLINI, M.L. A simulation environment for testing and research of neurally augmented fault tolerant control laws based on non-linear dynamic inversion, Proceedings of the AIAA Modeling and Simulation Technologies Conference, 2004, Providence, RI, USA.
23. FARMER, J., NORMAN, H., PACKARD, S. and PERELSON, A.S. The immune system, adaptation, and machine learning, *Physica* 22D 187-204, North-Holland, Amsterdam, Netherlands, 1986.
24. FORREST, S., PERELSON, A.S., ALLEN, L. and CHERUKURI, R. Self-nonsel self discrimination in a computer, Proceeding. of the IEEE Symposium on Research in Security and Privacy, IEEE Computer Society Press, Los Alamitos, CA, USA, 1994, pp 202-212.
25. DASGUPTA, D. and ATTOH-OKINE, N. Immunity-based systems: a survey, IEEE International Conference on Systems, Man, and Cybernetics, Orlando, Florida, USA, 1997.
26. BENJAMINI, E. *Immunology, A Short Course*, Wiley-Liss Publications, New York, NY, USA, 1992.
27. PERHINSCHI, M.G., CAMPA, G., NAPOLITANO, M.R., LANDO, M., MASSOTTI, L. and FRAVOLINI, M.L. Modeling and simulation of a fault tolerant control system, *Int J Modelling and Simulation*, January 2006, **26**, (1), pp 1-10.
28. PERHINSCHI, M.G. and NAPOLITANO, M.R. A simulation environment for design and testing of aircraft adaptive fault-tolerant control systems, *Aircraft Engineering and Aerospace Technology: An International Journal*, December 2008, **80**, (6), pp 620-632.
29. ANTONIEWICZ, R.F., DUKE, E.L. and PATTERSON, B.P. User's manual for interactive LINEAR, a Fortran program to derive linear aircraft models, NASA Technical Paper 2835, 1988.
30. CALISE, A.J. and SHARMA, M. Adaptive autopilot design for guided munitions, *AIAA J Guidance, Control and Dynamics*, 2000, **23**, (5).
31. Anonymous, Military Specification - Flying Qualities of Piloted Airplanes, US Department of Defense, MIL-F8785C, 1980.
32. LU, Y., SUNDARARAJAN, N. and SARATCHANDRAN, P. Analysis of minimal radial basis function network algorithm for real time identification of nonlinear dynamic systems', IEEE Proceedings on Control Theory and Application, 2000, **4**, (147), pp 476.
33. MONCAYO, H., PERHINSCHI, M.G. and DAVIS, J. Immunity - based aircraft failure detection and identification using an integrated hierarchical multi-self strategy, Proceedings of the AIAA Guidance, Navigation, and Control Conference, Chicago, IL, USA, August 2009.
34. GONZALEZ, F. and DASGUPTA, D. Anomaly detection using real-valued negative selection, *Genetic Programming and Evolvable Machines*, 2000, **4**, (4), pp 383-403, Kluwer.
35. GONZALEZ, F. and DASGUPTA, D. NIÑO, L. A randomised real-valued negative selection algorithm, Proceedings 2nd International Conference on Artificial Immune Systems, Edinburgh, UK, 2003, pp 261-272.
36. DAVIS, J., PERHINSCHI, M.G. and MONCAYO, H. Evolutionary algorithm for artificial immune system-based failure detector generation and optimisation, Proceedings of the AIAA Guidance, Navigation, and Control Conference, Chicago, IL, USA, August 2009.
37. SANCHEZ, S.P., PERHINSCHI, M.G., MONCAYO, H., NAPOLITANO, M.R., DAVIS, J. and FRAVOLINI, M.L. In-Flight Actuator Failure Detection and Identification for a Reduced Size UAV Using the Artificial Immune System Approach, Proceedings of the AIAA Guidance, Navigation, and Control Conference, Chicago, IL, USA, August 2009.